J Mater Sci (2011) 46:2733–2740
DOI 10.1007/s10853-010-5146-4

Martensitic transition and structural modulations in $Ni_{51}Fe_{24}Ga_{25}$ ferromagnetic shape-memory alloy

**Z. W. Du · B. L. Shao · A. S. Liu · G. H. Wu ·
J. F. Qian · Z. Y. Zhang · Z. Gao**

Received: 21 August 2010 / Accepted: 30 November 2010 / Published online: 14 December 2010

Abstract The structure of near-stoichiometric $Ni_{51}Fe_{24}Ga_{25}$ Heusler alloy synthesized by a melt-spinning technique has been studied using transmission electron microscopy. The main phase possessed a local, well-defined $L2_1$ high-atomic order structure, and some fcc structural γ phase and lamellar twin structures were also present. At room temperature, a rich variety of micro-modulated domains in the parent phase was observed. The domain structures were aligned along the $\langle 110 \rangle$, $\langle 100 \rangle$, $\langle 211 \rangle$, and $\sim 14°$ off $\langle 110 \rangle$ directions, resulting in a complex tweed contrast. These are possibly the precursors of martensitic transformation (MT). Below the MT temperature, Ms, the cubic parent phase transformed into modulated martensitic variants, which were composed of lamellar structures with predominantly 10 and 14 M modulated structures along the $\langle 110 \rangle$ directions.

Introduction

Shape-memory alloys (SMAs) have attracted much attention because of their potential application as smart materials [1, 2]. The ferromagnetic SMAs Ni–Mn–Ga alloy system is the most studied system from both applied and fundamental points of view [3–10]. However, due to their brittleness, other FSMA systems, such as Co–Ni–Ga [11], Ni–Co–Al [12], and Ni–Fe–Ga [13], are being investigated. The most studied aspects are the structure and magnetic transitions of Ni–Fe–Ga prepared using the conventional method [14–19]. However, unlike the extensively studied Ni–Mn–Ga system, Ni–Fe–Ga with low Ga content cannot be synthesized into the Heusler alloy phase by the conventional melting method because there is a strong competition between forming the γ solid solution phase and the intermetallic phase during the solidification process. On the other hand, adopting the melt-spun ribbon technique can prevent the γ solid solution phase and directly form the $L2_1$ phase. Liu et al. [20] have successfully synthesized Ni–Fe–Ga with a high atomic order $L2_1$ structure [14, 21] using this method. The structure and martensitic transformation (MT) of stoichiometric Ni_2FeGa FMSA prepared using this method has been studied through transmission electron microscopy (TEM) [22, 23].

In this paper, the structural properties and MT of non-stoichiometric $Ni_{51}Fe_{24}Ga_{25}$ alloy synthesized by a melt-spinning technique were studied using TEM and high-resolution electron microscopy (HREM). Structural modulations and MT were extensively analyzed. The field-induced strain in FMSAs is due to the influence of the field on the structural variants of martensite. Hence, a careful structural analysis, especially of the microstructural evolution based on MT, is important in understanding the significant properties of this new material.

Z. W. Du (✉) · B. L. Shao · A. S. Liu
General Research Institute for Nonferrous Metals,
Beijing 100088, China
e-mail: zhiweidu@126.com

G. H. Wu · J. F. Qian
State Key Laboratory for Magnetism, Institute of Physics,
Chinese Academy of Sciences, Beijing 100080, China

Z. Y. Zhang
Institute of Scientific and Technical Information of China,
Beijing 100038, China

Z. Gao
Department of Materials Science and Engineering,
Beijing University of Aeronautics and Astronautics,
Beijing 100083, China

Experimental procedures

The $Ni_{51}Fe_{24}Ga_{25}$ ribbon samples were synthesized by spinning the melted $Ni_{51}Fe_{24}Ga_{25}$ precursor ingot onto a high-speed cooling copper wheel. Experimental details of the sample preparation are the same as those reported in Ref. [20].

To determine the average structure, samples were characterized by X-ray diffraction (XRD, Philips X-pert diffractometer). The parent phase ($L2_1$) was subjected to MT under certain conditions of stress and strain. To avoid stress introduced from the grinding power, ribbons were directly used for XRD measurements. Similarly, during TEM sample preparation, 50–80 μm thick ribbons were selected for direct ion milling. TEM and HREM observations were carried out on a JEM-2000FX transmission electron microscope equipped with an energy dispersive X-ray spectroscopy (EDS) equipment, a Gatan cooling specimen holder, and a JEM-2010 high-resolution transmission electron microscope operated at 200 kV.

Results and discussion

Room temperature microstructure

Figure 1 shows the XRD pattern for the $Ni_{51}Fe_{24}Ga_{25}$ ribbons at room temperature (RT). All intense peaks can be indexed to a $L2_1$ structure with calculated lattice parameters of $a = b = c = 5.74$ Å and $\alpha = \beta = \gamma = 90°$. The characteristic peaks also reveal a small amount of fcc structural γ phase with the lattice parameter $a = 3.6$ Å.

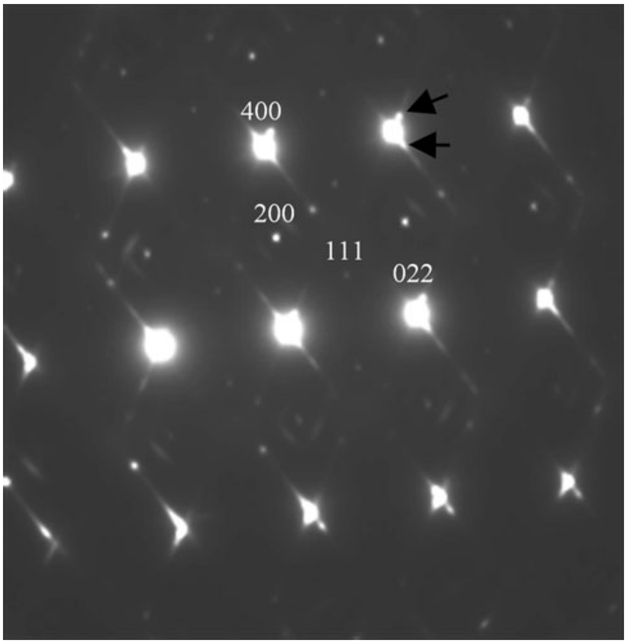

Fig. 2 SAED pattern along the $[01\bar{1}]$ zone axis; the (111) diffraction spots reveal the $L2_1$ structure feature of the $Ni_{51}Fe_{24}Ga_{25}$ alloy

To understand the structural details of the as-prepared specimens, TEM and HREM analyses were further carried out.

Specimens selected from segments of different ribbons in the same state were observed. TEM analysis reveals a uniform microstructure of specimens, which have a mainly local, well-defined $L2_1$ order structure. Figure 2 shows the selected area electron diffraction (SAED) pattern taken along the $[01\bar{1}]$ zone axis direction. The appearance of

Fig. 1 XRD pattern for the $Ni_{51}Fe_{24}Ga_{25}$ alloy at room temperature

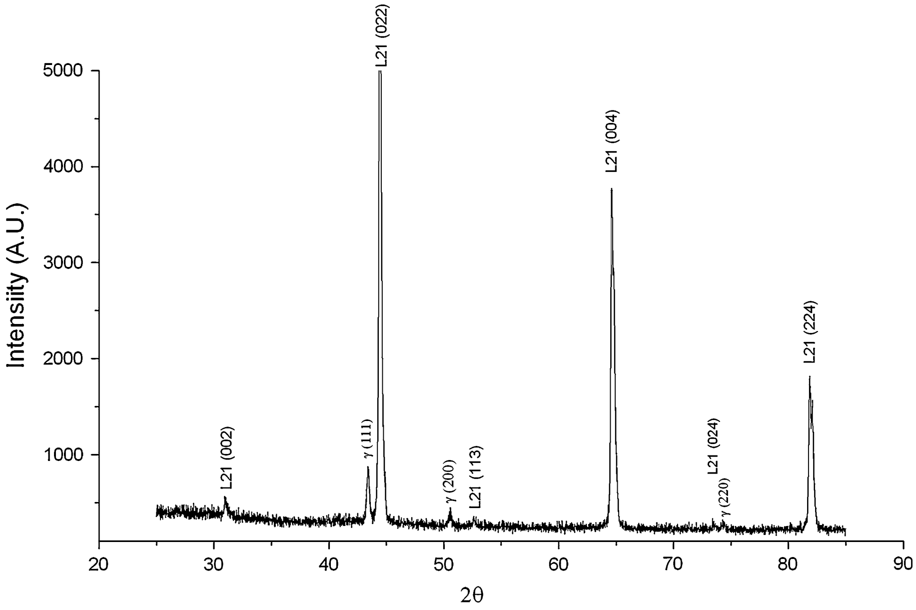

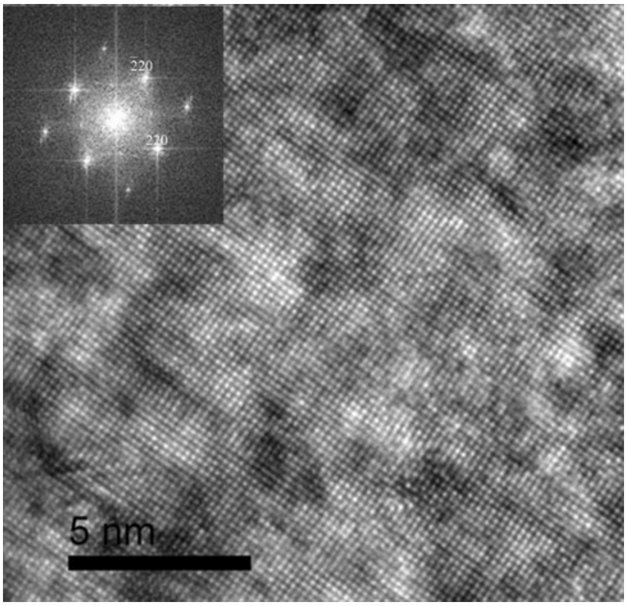

Fig. 3 HREM image taken along the [001] zone axis exhibits an atomic order L2_1 structure

(111) diffraction spots in the pattern suggests a well-defined L2_1 chemical order (Heusler phase) [22, 23] in the current system. Figure 3 shows an HREM image taken along the [001] zone axis. The inset is the corresponding fast Fourier transformation (FFT) image, which further suggests a perfect L2_1 structure. However, in a certain specimen, a small amount of twin microstructures with unknown structural parameters exist (Fig. 4). A small amount of γ phase (marked by the arrow in Fig. 5a) was also detected in some specimens. The lattice parameter calculated from the SAED pattern in Fig. 5b agrees with the XRD results.

Figure 6 represents a set of typical SAED patterns frequently observed along the [001] zone axis at RT. Besides the main diffraction spots of the $L2_1$ structure, additional satellites and diffuse streaks can also be observed. These are frequently present in a single SAED pattern with different configurations. Figure 6a–c shows sets of satellites with different configurations. Figure 6d and e simultaneously shows satellites and paired diffuse streaks.

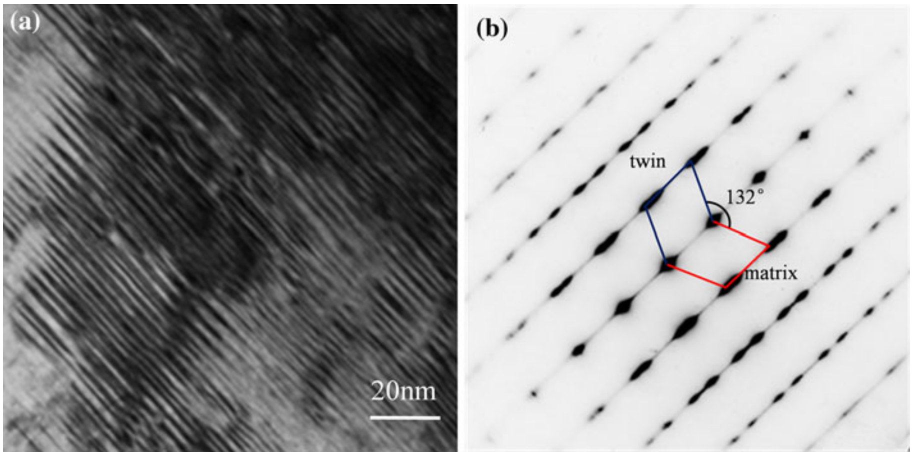

Fig. 4 Bright field (BF) image (**a**) and the corresponding SAED pattern (**b**) of a lamellar twin microstructure

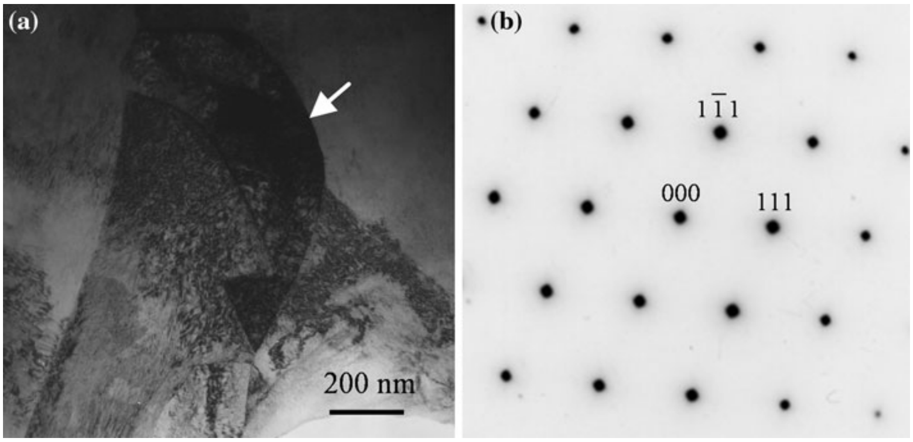

Fig. 5 BF image (**a**) and SAED pattern (**b**) indicate the presence of an fcc structural γ phase

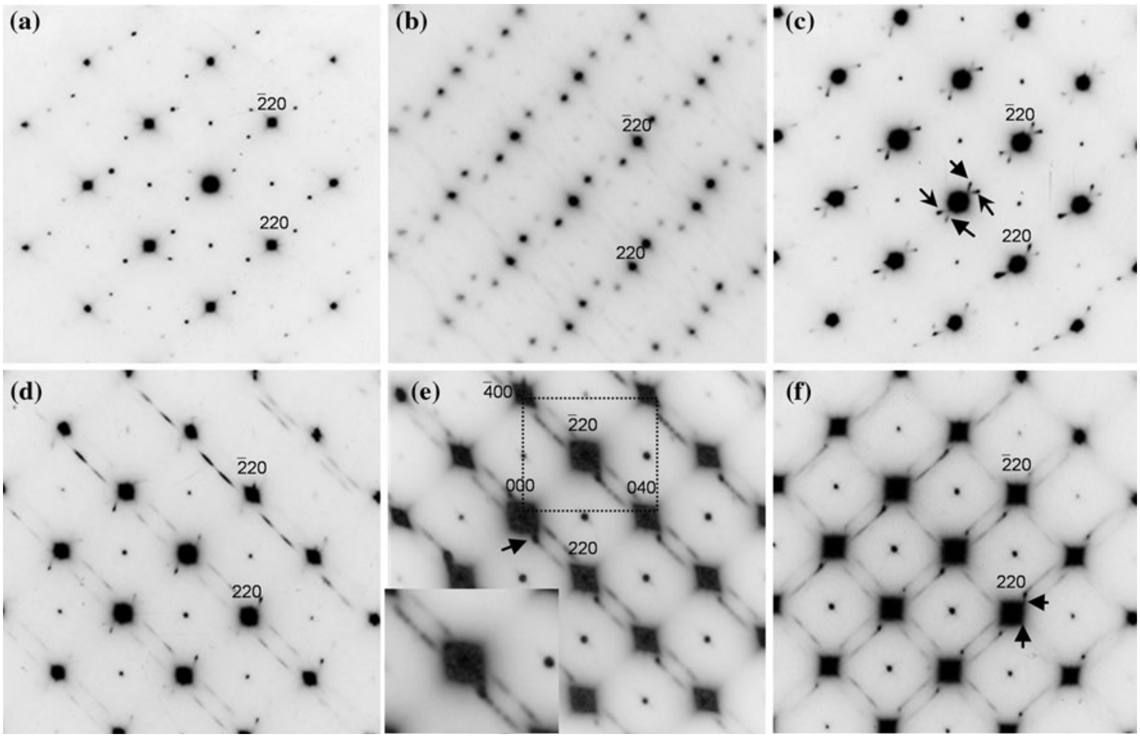

Fig. 6 SAED patterns along the [001] zone axis exhibiting micro-modulated structures in the as-prepared sample at room temperature: **a–c** showing three different configurations of the satellites. **d–f** showing paired diffuse streaks running symmetrically perpendicular to the $\langle 110 \rangle$ directions

The main diffraction spots are regularly surrounded by satellites and diffuse streaks. The former can be expressed by an additional modulation wave vector $\pm(\pm k_1[220] + k_2[\bar{2}20])$ (as indicated by arrows in Fig. 6c) and $\pm(k_2[220] \pm k_1[\bar{2}20]20)$ (as indicated by arrows in Fig. 6e), where k_1 (~ 0.064) and k_2 (~ 0.266) are calculated by the average of the measured results. The small difference in k_1 in Fig. 6a–c is attributed to the slightly off-the-zone axis and the Ewald sphere effect. The spatial positions of the satellites are $\sim 14°$ off the $[\bar{2}20]$ direction. The regularly distributed satellites suggest that a structural modulation along $\sim 14°$ off the $\langle 110 \rangle$ direction exists in the austenite phase.

Figure 6d and e represents much clearer paired diffuse streaks running symmetrically perpendicular to the $\langle 110 \rangle$ direction. The inset in Fig. 6e shows an enlarged image of the diffuse streaks between (040), $(\bar{4}00)$, and $(\bar{2}20)$ reflections. The streaks are composed of a series of diffuse satellites, which suggests a multi-modulated structure with a different modulation wave vector, q. Moreover, the starting points of the streaks are located at almost the same positions as the satellites. This indicates that the multi-modulated structure has a minimum modulation wave vector, $q_{\min}$ (corresponding to the maximum modulation period), which is equivalent to the modulation wave vector of the satellites.

Besides the additional satellite spots and diffuse streaks mentioned, diffuse satellites superimposing streaks along both the $\langle 110 \rangle$ and $\langle 211 \rangle$ directions are also observed (indicated by arrows in Figs. 2; 6f). This suggests that structural modulations along the $\langle 110 \rangle$ and $\langle 211 \rangle$ directions are also present. In a previous study on Ni_2FeGa, the same kind of structural modulation has also been found [22]. Diffuse diffractions along the $\langle 110 \rangle$ direction are considered related to the phonon anomaly in the $[\zeta\zeta 0]$ TA_2 branch of the Heusler phase.

To sum up, the abundance of SAED patterns suggests that many microstructures exist in the Ni_2FeGa alloy. A rich variety of micro-domains has been observed at RT in the as-prepared samples. Striations lie along the $\langle 100 \rangle$ direction (Fig. 7a). Tweeds of several nanometers composed of micro-domains along the $\langle 110 \rangle$ and $\langle \bar{1}30 \rangle$ directions are shown in Fig. 7b. In addition, micro-domains along two directions with a habit plane angle of about 28° and ±14° off the $\langle 110 \rangle$ direction are shown in Fig. 7c. These are related to the spatial position of the satellites and the starting points of the streaks shown in Fig. 6. The fine structure of the tweeds shown in Fig. 7c was further analyzed by HREM. Figure 8a shows the HREM and corresponding FFT pattern that contain paired diffuse streaks. Figure 8b is the inverse FFT (IFFT) image filtered using

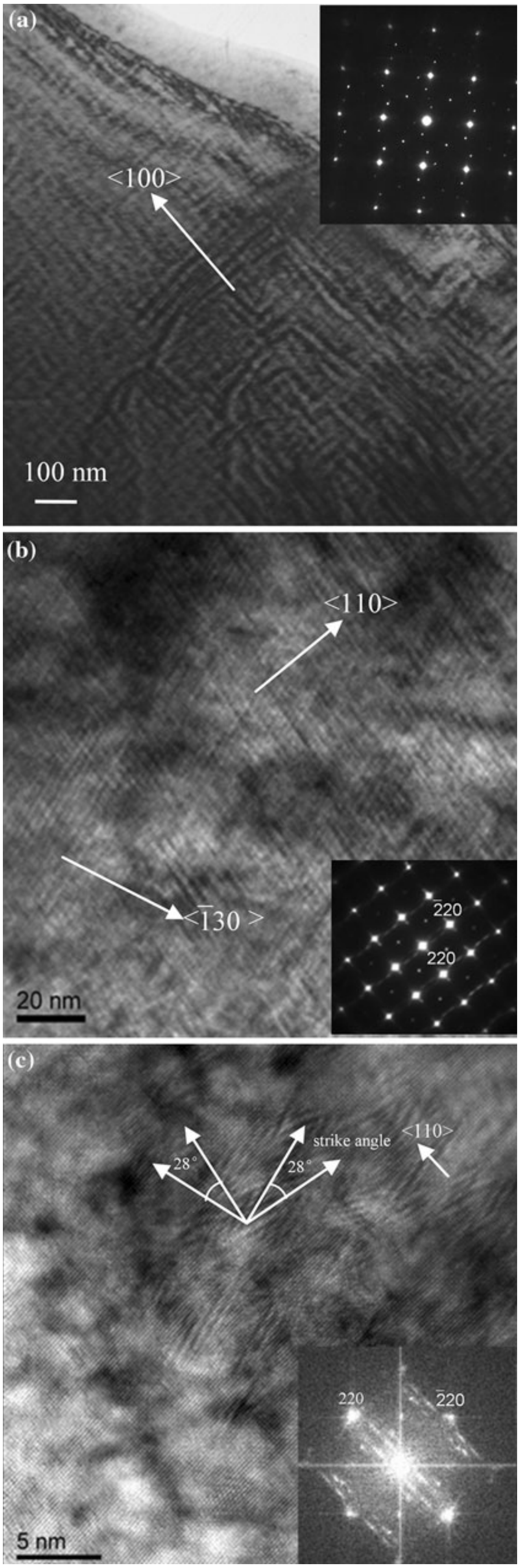

Fig. 7 **a–c** A variety of micro-domains with tweed contrast present in the $Ni_{51}Fe_{24}Ga_{25}$ alloy at RT

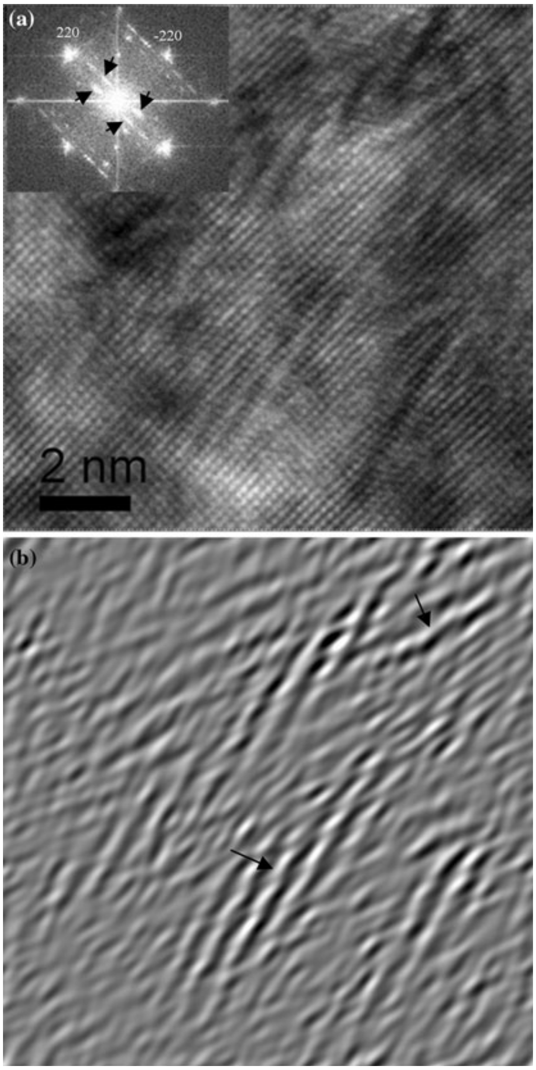

Fig. 8 **a** HREM image taken with the incident beam along [001] and the corresponding FFT image. **b** IFFT image filtered using the streaks indicated by the *arrows* in **a**

the paired streaks indicated by arrows in Fig. 8a. Long period modulation structures with slightly different modulation wavelengths are clearly revealed by the fringes (indicated by arrows in Fig. 8b). The fluctuation of the fringes reveals the multi-modulation and lattice distortion from the average structure.

Figure 9 shows a $[1\bar{1}1]$ zone axis HREM image. The long period structure along the $\langle 110 \rangle$ direction further indicates the existence of structural modulation along the $\langle 110 \rangle$ direction in the parent phase. In addition, evident structural distortions, corresponding to atomic displacement from the standard position, are also visible. Figure 10 shows a typical [001] zone axis HREM image. The corresponding FFT shows paired diffuse streaks running around the main diffraction spots. In most areas, the square

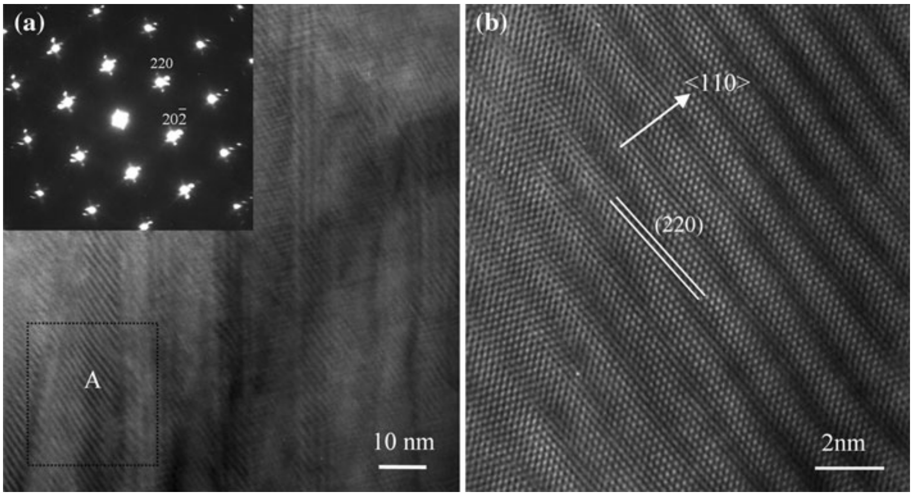

Fig. 9 **a** BF image along the $[1\bar{1}1]$ zone axis and the corresponding SAED pattern, **b** HREM image corresponding to *marked area A* in **a**, exhibiting structural modulation along the ⟨110⟩ direction (long period structure) in the parent phase

lattices have been transformed into oblique lattices. Therefore, lattice distortions indicate the kinds of modulated structures in the current system. These areas with oblique lattices are possibly the precursors of martensitic variants below Ms.

Low-temperature MT

To understand the MT of the $Ni_{51}Fe_{24}Ga_{25}$ alloy, in situ cooling TEM observations were performed from RT to −163 °C. Several samples have been observed and the areas near the ⟨001⟩ and ⟨110⟩ zone axes were selected to record MT. The lamellar martensitic phase in the current system begins to appear at around −80 °C. The diffuse satellites change progressively toward superstructure spots with decreasing temperature. After being held at about −160 °C for a long time, the SAED pattern with $L2_1$

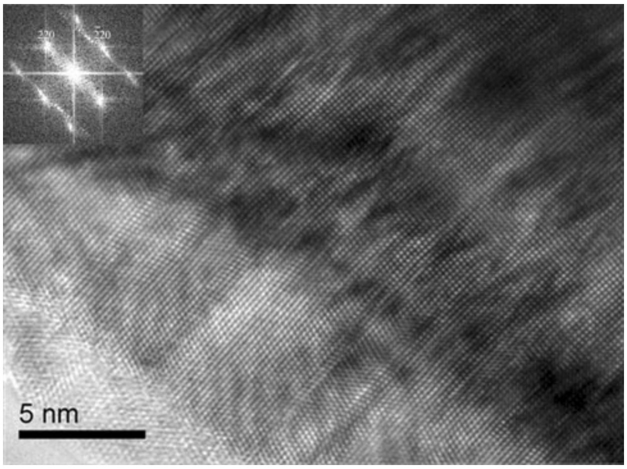

Fig. 10 HREM image taken along the [001] zone axis and the corresponding FFT image. In most areas, the square lattices are transformed into oblique lattices

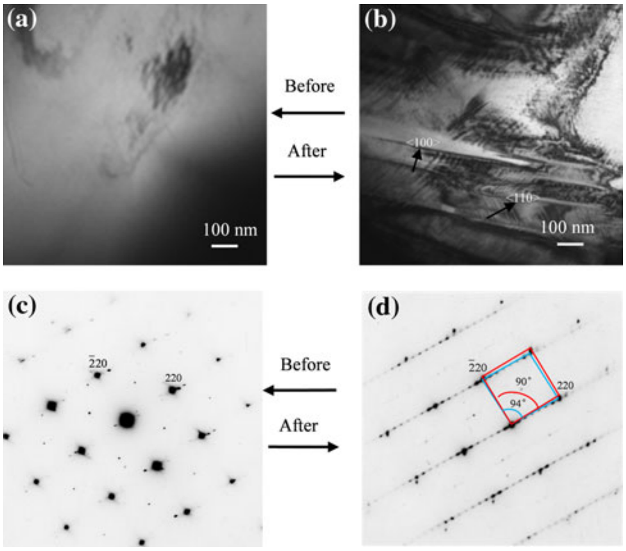

Fig. 11 BF image (**a**, **b**) and the corresponding SAED patterns (**c**, **d**) for $Ni_{51}Fe_{24}Ga_{26}$ before and after 14 M MT

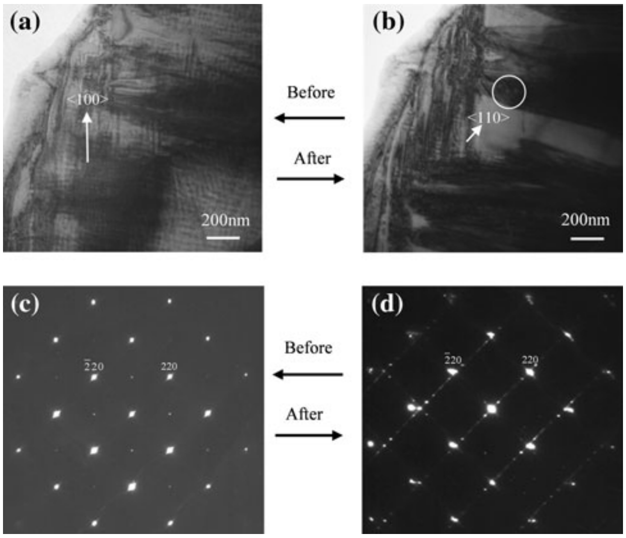

Fig. 12 BF image (**a**, **b**) and the corresponding SAED patterns (**c**, **d**) for $Ni_{51}Fe_{24}Ga_{26}$ before and after 10 M MT

structural main diffraction spots, superimposing additional spots and streaks, finally transforms to several typical superstructures. Figure 11 shows a typical change in the bright field (BF) image and corresponding SAED pattern with MT. For convenience, the diffraction spots are indexed by reference to the cubic parent phase. The superstructure appears along the ⟨110⟩* direction (Fig. 11d) with a wave vector of (2a* + 2b*)/7, which has a planar distance seven times {220} the plane distance. Conventionally, it is called a seven-layer (or 14 M) modulated martensite. Another remarkable structural feature in the low-temperature martensite is the appearance of a 10 M modulation along the ⟨110⟩* direction, with a wave vector of (2a* + 2b*)/5 (Fig. 12d). The SAED patterns either in Figs. 11d or 12d are composed of two sets of diffraction spots. One set has a 90° angle between the nearest two reciprocal vectors (Fig. 11d). The diffraction spots are attributed to the original $L2_1$ phase (Fig. 11c) in the

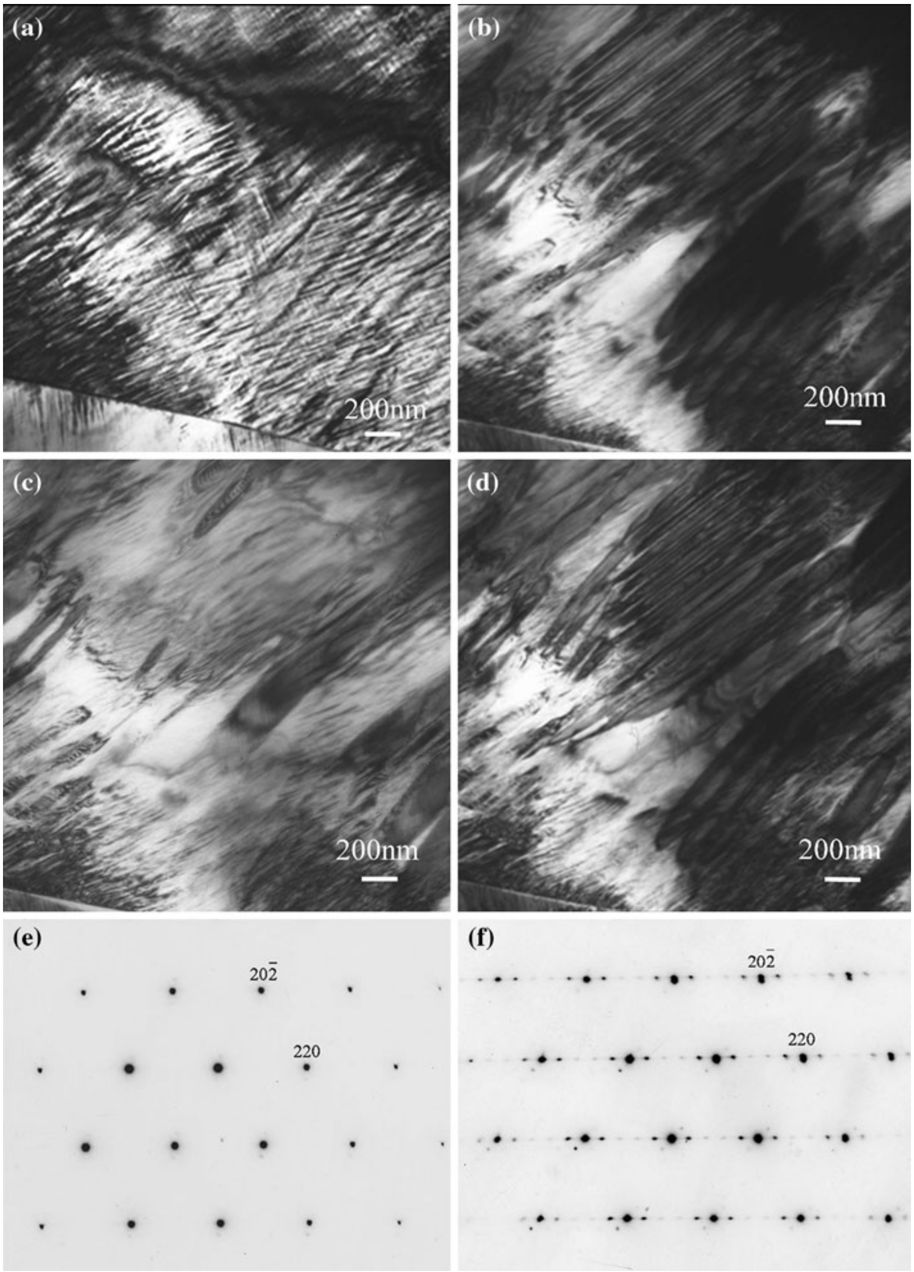

Fig. 13 BF image and the corresponding SAED patterns, exhibiting a repeated contrast change for $Ni_{51}Fe_{24}Ga_{26}$ during MT. **a** Tweeds in the parent phase, **b** martensitic laths appear under Ms, **c** martensitic laths disappear abruptly, **d** martensitic laths reappear again, **e** and **f** SAED patterns corresponding to **a** and **b**

residual austenite. Another set with a 94° angle between the nearest two reciprocal vectors corresponds to a 14 M modulated martensite structure along the $\langle 110 \rangle$ direction (Fig. 11d). Similarly, Fig. 12d shows the 10 M modulated martensite. The direction of the primary laths is almost consistent with the tweeds of the parent phase along the $\langle 100 \rangle$ direction and the secondary laths along the $\langle 110 \rangle$ direction (Figs. 11b; 12b), which suggests that the tweeds in the parent phase are related to the MT.

During MT, the contrast of BF image changes repeatedly. As shown in Fig. 13, the lamellar structures appear (Fig. 13b) at a certain time, disappear abruptly (Fig. 13c), and then reappear (Fig. 13d). This process is frequently observed. It could be due to a change in the imaging conditions caused by a change in the orientation of the thin foil. During in situ experiments, the thin foil orientation is continuously changing due to thermal dilatation effects and the MT strain. This is specially enhanced when a martensite plate is formed in a place close to the observation area; the shear strain of this plate usually causes an abrupt change of the orientation of the observation area that could lead to the invisibility of the defects.

Conclusions

TEM observations and XRD analyses reveal that the main phase in specimens possesses a local, well-defined $L2_1$ high-atomic order structure. Moreover, a small amount of twin microstructures with an unknown structural parameter and a small amount of fcc structural γ phase with the lattice parameter $a = 3.6$ Å are also present. SAED patterns, BF images, and HREM images exhibit a rich variety of structurally micro-modulated domains in the parent phase at RT. The domain structures are aligned along the $\langle 110 \rangle$, $\langle 100 \rangle$, $\langle 211 \rangle$, and 14° off $\langle 110 \rangle$ direction, resulting in a complex tweed contrast. HREM images reveal lattice distortion, which shows the kinds of structural modulations in the current system. The modulated domains are possible precursors of MT. Below Ms, the cubic parent phase transforms into modulated martensitic variants with little residual austenite. The modulated martensitic variants have a lamellar structure, which are predominately 10 and 14 M superstructures along the $\langle 110 \rangle$ directions. The directions of the micro-domains in the parent are related to that of the martensitic variants.

Acknowledgement This work is supported by the National Science Foundation of China with Grant No. 50801007 and 50971130.

References

1. Eskil M, Ceylan M (2009) J Mater Sci 44:3633. doi:10.1007/s10853-009-3469-9
2. Coughlin J, Williams J, Chawla N (2009) J Mater Sci 44:700. doi:10.1007/s10853-008-3188-7
3. Ullakko K, Huang JK, Kantner C (1996) Appl Phys Lett 69:1966
4. Wu GH, Yu CH, Meng LQ (1999) Appl Phys Lett 75:2990
5. Pons J, Chernenko VA, Santamarta R (2000) Acta Mater 48:3027
6. Sozinov A, Likhachev AA, Lanska N, Ullakko K (2002) Appl Phys Lett 80:1746
7. Bennett JC, Hyatt CV, Gharghouri MA (2004) Mater Sci Eng A 378:409
8. Pons J, Santamarta R (2003) Mater Chem Phys 81:457
9. Dong GF, Gao ZY, Tan CL (2010) J Mater Sci 45:5490. doi:10.1007/s10853-010-4606-1
10. Prasad RVS, Phanikumar G (2009) J Mater Sci 44:2553. doi:10.1007/s10853-009-3333-y
11. Wuttig M, Li J, Craciunescu C (2001) Scr Mater 44:2393
12. Oikawa K, Wulff L, Ijima T, Gejima F, Ohmori T, Fujita A (2001) Appl Phys Lett 79:3290
13. Oikawa K, Ota T, Ohmori T, Tanaka Y, Morito H, Fujita A (2002) Appl Phys Lett 81:5201
14. Hamilton RF, Sehitoglu H, Efstathiou C, Maier HJ (2007) Acta Mater 55:4867
15. Omori T, Kamiya N, Sutou Y, Oikawa K, Kainuma R, Ishida K (2004) Mater Sci Eng A 378:403
16. Picornell C, Pons J, Cesari E, Dutkiewicz J (2008) Intermetallics 16:751
17. Santamarta R, Cesari E, Font J, Muntasell J, Pons J, Dutkiewicz J (2006) Scr Mater 54:1985
18. Seguí C, Pons J, Cesari E, Dutkiewicz J (2006) Mater Sci Eng A 438–440:923
19. Barandiarán JM, Gutiérrez J, Lázpita P, Chernenko VA (2008) Mater Sci Eng A 478:125
20. Liu ZH, Zhang M, Cui YT, Zhou YQ, Wang WH, Wu GH, Zhang XX, Xiao G (2003) Appl Phys Lett 82:424
21. Liu ZH, Hu HN, Liu GD, Cui YT, Zhang M, Chen JL, Wu GH (2004) Phys Rev B 69:134415
22. Li JQ, Liu ZH, Yu HC, Zhang M, Zhou YQ, Wu GH (2003) Solid State Commun 126:323
23. Zhang HR, Ma C, Tian HF, Wu GH, Li JQ (2008) Phys Rev B 77:214106